APL Photonics

Programmable omni-resonance using space–time fields

Abbas Shiri, (iD) Kenneth L. Schepler, and (iD) Ayman F. Abouraddy

View Online   Export Citation   CrossMark

ARTICLES YOU MAY BE INTERESTED IN

Tubular optical microcavities based on rolled-up photonic crystals
APL Photonics 5, 106106 (2020); https://doi.org/10.1063/5.0022862

Reciprocity-induced symmetry in the round-trip transmission through complex systems
APL Photonics 5, 106104 (2020); https://doi.org/10.1063/5.0021285

Nanophotonic source of quadrature squeezing via self-phase modulation
APL Photonics 5, 101303 (2020); https://doi.org/10.1063/5.0024341
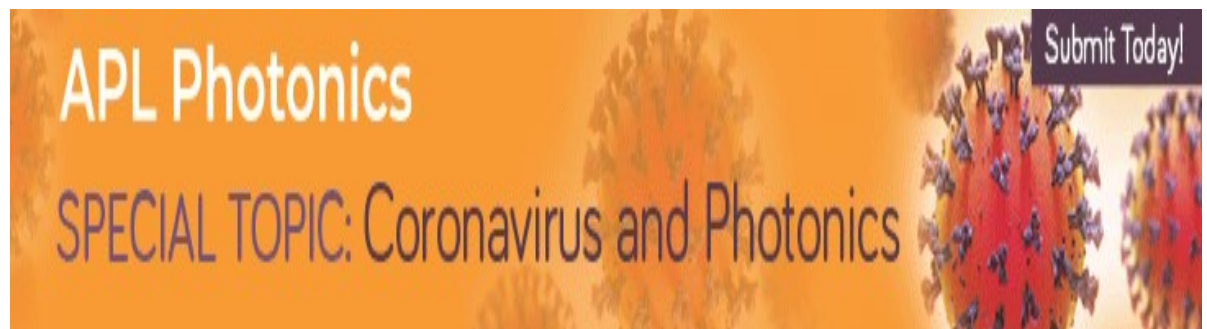
AIP Publishing

Programmable omni-resonance using space–time fields

View Online   Export Citation   CrossMark

Abbas Shiri,[1,2] Kenneth L. Schepler,[1] (iD) and Ayman F. Abouraddy[1,2,a] (iD)

AFFILIATIONS

[1] CREOL, The College of Optics and Photonics, University of Central Florida, Orlando, Florida 32816, USA
[2] Department of Electrical and Computer Engineering, University of Central Florida, Orlando, Florida 32816, USA

[a]Author to whom correspondence should be addressed: raddy@creol.ucf.edu

ABSTRACT

Omni-resonant wave packets are pulsed optical beams that couple to planar cavities even when the wave packet bandwidth far exceeds the cavity resonant linewidth by virtue of a precise spatiotemporal structure introduced into the optical field. We demonstrate experimentally the synthesis of *programmable* omni-resonant wave packets in which a prescribed pulse spectrum is made to resonate with a planar cavity. Examples include controllable-bandwidth resonant spectral lines, spectral holes with tunable notch bandwidth, and even arbitrary resonant spectra. These novel resonant interactions are realized with no changes made to the cavity itself, and therefore, without compromising its quality factor—only sculpting the spatiotemporal spectrum of the incident field is required. Programmable omni-resonance allows harnessing resonant field enhancements over arbitrary spectral profiles without restriction to traditionally narrow resonant linewidths.

I. INTRODUCTION

Optical resonators, an indispensable component in the photonics purview,[1] are essential for the construction of lasers, gyroscopes, and establishing classical and quantum light–matter interfaces,[2] among a plethora of other applications. Associated with optical resonances is a field enhancement that typically occurs only over narrow spectral linewidths at discrete resonant wavelengths. As the quality factor of the resonator increases, field build-up is *boosted*, thereby leading to the enhancement of optical effects (such as resonant absorption[3–7] and nonlinear optical effects[8–12]). Inevitably, however, the linewidth over which this boosted enhancement is harnessed concomitantly *decreases*. Fundamentally, this inverse relationship is due to the link between the cavity-photon lifetime and the resonant linewidth.[1] In an attempt to overcome this restriction, previous efforts have aimed at constructing "white-light" cavities in which the resonant linewidth is increased without sacrificing the cavity quality factor.[13] This has been realized by introducing anomalous dispersion into the cavity, e.g., inserting an atomic gas[14,15] or exploiting nonlinear resonances.[16] It is now well-established that incorporating linear passive optical components into a cavity (such as gratings[17] or chirped Bragg reflectors[18]) cannot satisfy the

conditions for a white-light cavity and that only the addition of an active medium into the cavity provides the requisite anomalous dispersion.

A recently emerging alternative strategy to enhance the resonant linewidth of a planar cavity *without* modifying the cavity or compromising its quality factor is to sculpt the spatiotemporal structure of the incident field, which we have termed "omni-resonance." A planar Fabry–Pérot (FP) cavity can be viewed as a device that presents a particular form of angular dispersion,[19] in which each resonance corresponds to a curved trajectory in the angular–spectral domain. Such a device-induced spatiotemporal coupling can be neutralized by judiciously introducing opposing angular dispersion into the incident field, thereby transforming the pulsed field into a so-called "space–time" (ST) wave packet.[20–24] By associating each wavelength with a single spatial frequency,[25] these ST wave packets then become omni-resonant: they can couple fully to a single resonance even if the bandwidth of the ST wave packet is substantially wider than the resonant linewidth.[26] The wave packet can then traverse the cavity without a change in the spectrum or spatial profile after resonating with the cavity over a broad continuous spectrum.[27,28]

Here, we show that the spatiotemporal spectral correlations imparted to an optical field using a spatial light modulator can

be exploited to program the omni-resonance. Wavelengths can be selectively eliminated from the resonant spectrum by associating them with spatial frequencies that do not provide the requisite angular dispersion to resonate with the cavity. Examples of programmable omni-resonant ST wave packets we synthesize include resonances with controllable bandwidth (narrower or wider than the cavity native resonant linewidth), spectral holes of controllable bandwidth notched into a broad omni-resonant spectrum, and arbitrary spectral profiles induced to resonate with the cavity. By severing the fundamental link between the cavity-photon lifetime and the resonant bandwidth,[1] these results suggest a host of potential applications that harness resonant field enhancements in linear and nonlinear photonic devices for sensing, filtering, and lasing.

II. PROGRAMMABLE OMNI-RESONANCE

A. Basic concept

The concept of programmable omni-resonance is illustrated in Fig. 1. Consider a broadband collimated coherent field (an ultrashort pulse in the time domain) normally incident on a planar symmetric FP cavity comprising two symmetric mirrors separated by a layer of index n and thickness d. Only narrow linewidths centered at the resonant free-space wavelengths $\lambda_m(0) = 2nd/m$ are transmitted, where integer m is the resonance order [Fig. 1(a)]. At oblique incidence, at an external angle ϕ (with respect to the normal to the cavity), the resonances $\lambda_m(\phi)$ are *blue*-shifted,

$$\lambda_m(\phi) = \lambda_m(0)\sqrt{1 - \frac{1}{n^2}\sin^2\phi} < \lambda_m(0). \qquad (1)$$

This equation represents the spatiotemporal dispersion relationship of the mth cavity resonance, corresponding to the (k_x, λ)-space dotted curves in Fig. 1 (bottom panels).

If this pulsed field is focused into the FP cavity with a cylindrical lens, each incident wavelength becomes associated with a broad range of external incident angles ϕ [Fig. 1(b)]. The transmitted field corresponds to the intersection of the incident field's spatiotemporal spectrum (which is separable with respect to wavelength λ and angle
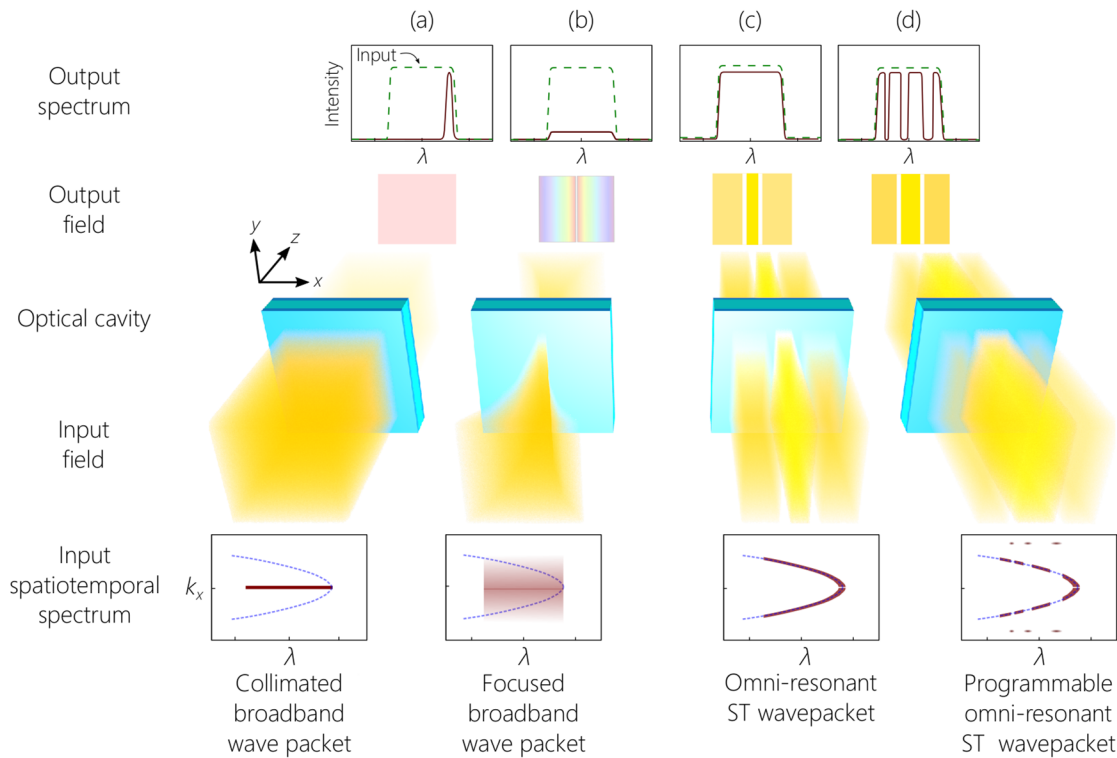
FIG. 1. Concept of programmable omni-resonance. (a) A collimated broadband optical field is incident on a planar FP cavity. The input spatiotemporal spectrum $\widetilde{E}(k_x, \lambda) = \widetilde{E}(\lambda)\delta(k_x)$ is separable with respect to the spatial and temporal degrees of freedom. The dotted curve in the bottom panel is the spatiotemporal spectrum [the collection of plane waves described by (k_x, λ) pairs] for a single resonance of the FP cavity; the solid region is the spatiotemporal spectrum of the input field $\widetilde{E}(k_x, \lambda)$. The output is the usual spectrally narrow linewidth centered at a resonant wavelength. (b) A focused broadband beam allows for a fraction of the power at each wavelength to traverse the cavity. The input spatiotemporal spectrum is still approximately separable. The output spectrum retains the input profile but with a strongly reduced amplitude because each wavelength is resonant at only one angle of incidence and is rejected at all other angles. (c) An omni-resonant ST wave packet traverses the FP cavity without a change in its bandwidth (even when much wider than the resonant linewidth) by virtue of its spatiotemporal spectrum—no longer separable with respect to k_x and ω—matching that of the cavity resonance. (d) By tailoring the spatiotemporal spectrum of the input field, programmable omni-resonance is achieved. Selectively displacing wavelengths at the input from the spatiotemporal spectrum associated with omni-resonance enables sculpting the transmitted optical spectrum independently of the resonant linewidth.

of incidence ϕ) with the resonant dispersion relationship in Eq. (1). Consequently, only a small fraction of the power emerges from the cavity across the whole spectrum [Fig. 1(b)], with each wavelength emerging at a distinct angle. As such, faint colored bands appear in the collimated output field.[1]

Omni-resonance[26–28] refers to the field configuration whereupon each wavelength λ in the pulse is arranged to be incident on the cavity at a different angle $\phi(\lambda)$ [Fig. 1(c)]. It is convenient to consider the spatial frequency $k_x(\lambda) = \frac{2\pi}{\lambda}\sin\phi(\lambda)$, the transverse component of the wave vector along the transverse coordinate x, *in lieu* of the angle of incidence ϕ. By modifying the spatiotemporal spectrum of the pulse to associate each wavelength with a specific spatial frequency $k_x(\lambda)$ satisfying Eq. (1), the incident pulse is transformed into an omni-resonant ST wave packet.[23,25] Matching the spatiotemporal spectrum of the omni-resonant ST wave packet to the resonance spatiotemporal dispersion curve allows a continuous spectrum to couple to the mth resonance[28] when all wavelengths simultaneously satisfy the condition

$$\sin\phi(\lambda) = n\sqrt{1 - (\lambda/\lambda_m(0))^2}. \tag{2}$$

If λ deviates from the resonant wavelength $\lambda_m(0)$ by $\Delta \ll \lambda_m(0)$, where $\lambda = \lambda_m(0) - \Delta$, then $\sin\phi(\lambda) \approx n\sqrt{2\Delta/\lambda_m(0)}$. Because each incident wavelength across the entire continuous omni-resonant spectrum is fully coupled to the cavity resonance,[26,28] the output spectrum matches that of the input *without* reduction in amplitude [Fig. 1(c)].

Programmable omni-resonance refers to the possibility of sculpting the resonating spectrum in the cavity through tailoring the spatiotemporal spectrum of the incident field—independently of the resonant linewidth [Fig. 1(d)]. Displacing undesired wavelengths from the spatiotemporal omni-resonant spectral loci prevents these wavelengths from coupling into the cavity, and they, instead, reflect back from it. The rest of the spectrum—which can take on an arbitrary profile—couples to the target cavity resonance, thereby realizing a programmable omni-resonant ST wave packet [Fig. 1(d)]. As such, the same cavity can be exploited in a variety of resonant configurations without compromising its quality factor, indeed without modifying the cavity itself in any way. We proceed to synthesize programmable omni-resonant ST wave packets experimentally and demonstrate a variety of unique resonant spectral realizations.

III. EXPERIMENT

The cavity used in our demonstrations of programmable omni-resonance comprises a 10-μm-thick silica spacer sandwiched between two Bragg mirrors consisting of eight bilayers of SiO_2 (138-nm-thick, refractive index $n = 1.46$ at a wavelength of 800 nm) and TiO_2 (88-nm-thick, $n = 2.28$ at 800 nm), deposited on a glass substrate. The cavity-free spectral range is $\approx$22 nm, as measured by using a broadband white-light source (Thorlabs QTH10, Quartz Tungsten-Halogen Lamp) and collecting the transmitted light with a multimode fiber (300-μm-diameter, 0.39 NA; Thorlabs M69L02) connected to a spectrometer (Jaz, Ocean Optics). The cavity linewidth is $\approx$0.15 nm, as measured using a mode-locked femtosecond Ti:sapphire laser and collecting the transmitted light

with a single-mode fiber (Thorlabs P1780A-FC) and high-resolution optical spectrum analyzer (OSA; ANDO AQ6317B).

Synthesis of the ST wave packets [Fig. 2(a)] starts with 100-fs pulses from a Ti:sapphire laser centered on a wavelength of $\approx$800 nm that are directed to a diffraction grating (Newport 10HG1200-800-1, 1200 lines/mm, area 25×25 mm^2) to spread the spectrum in space before a cylindrical lens (focal length $f = 500$ mm) collimates the spectrum and directs it to a spatial light modulator (SLM; Hamamatsu X10468-02). The SLM assigns to each wavelength a linear phase variation along x corresponding to a prescribed spatial frequency k_x. The modulated wave front is retro-reflected back to the grating that reconstitutes the pulse and produces the ST wave packet. The spectrum of the Ti:sapphire laser gets filtered by the physical size of the SLM to a bandwidth of 1.5 nm (from 797.1 nm to 798.6 nm, the longest wavelength in this range corresponds to a cavity resonance at normal incidence). Two cylindrical lenses then introduce a demagnification factor of $\times$10 before impinging on the FP cavity,
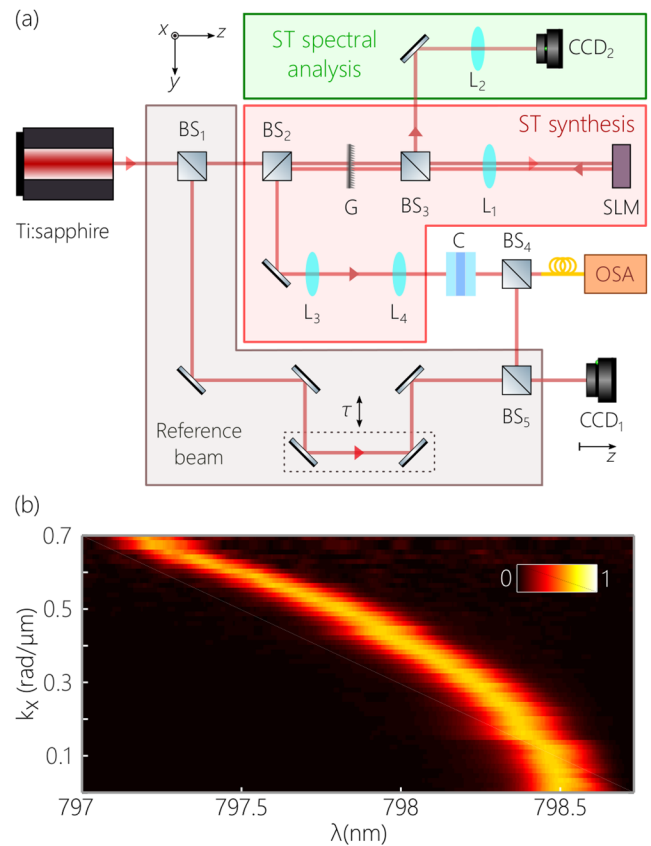
FIG. 2. (a) Schematic of the experimental arrangement. G: diffraction grating; L: lens; BS: beam splitter; SLM: spatial light modulator; C: FP cavity; OSA: optical spectrum analyzer; CCD: charged-coupled device camera. CCD_1 captures the time-averaged intensity of the ST wave packet when the reference arm is blocked and otherwise records the interference of the ST wave packet with the reference pulse. CCD_2 captures the spatiotemporal spectrum of the ST wave packet. (b) Measured spatiotemporal spectrum of a single resonance of the FP cavity used in our experiments.

which is placed on a rotation stage ≈3 cm from L_4. The wave packet transmitted through the cavity is then collected with a multi-mode fiber (50-μm-diameter, 0.22-NA, Thorlabs M42L01) and delivered to the OSA.

IV. REALIZING PROGRAMMABLE OMNI-RESONANCE

We start by measuring the angular dispersion of the FP cavity [Fig. 2(b)]. When the SLM imparts a uniform phase distribution to the spectrally resolved impinging field, all the wavelengths are assigned to a fixed angle of incidence $\phi = 0$ ($k_x = 0$); see Figs. 3(a–i), 3(b–i), and 3(c–i). The measured transmitted spectrum [Fig. 3(d–i)] matches the normal-incidence cavity resonance. When the SLM imparts to all the incident wavelengths a linear phase distribution

(modulo 2π) corresponding to a particular spatial frequency k_x, oblique incidence is realized [Figs. 3(a–ii), 3(b–ii), and 3(c–ii)] with a blue-shifted resonance [Fig. 3(d–ii)], as expected from Eq. (1). By scanning through values of k_x (or angle of incidence ϕ), we can reconstruct the spatiotemporal dispersion curve of the selected cavity resonance in (λ, k_x) space [Fig. 2(b)].

An omni-resonant ST wave packet is synthesized by associating each wavelength λ at the SLM with the appropriate spatial frequency $k_x(\lambda)$ that results in that wavelength resonating with the cavity according to Eq. (2) [Fig. 3(a–iii)]. The requisite phase distribution imparted by SLM is shown in Fig. 3(b–iii), resulting in the measured spatiotemporal spectrum of the ST wave packet in Fig. 3(c–iii) that matches the spatiotemporal spectrum of the cavity resonance [Fig. 2(b)]. Consequently, the spectrum transmitted
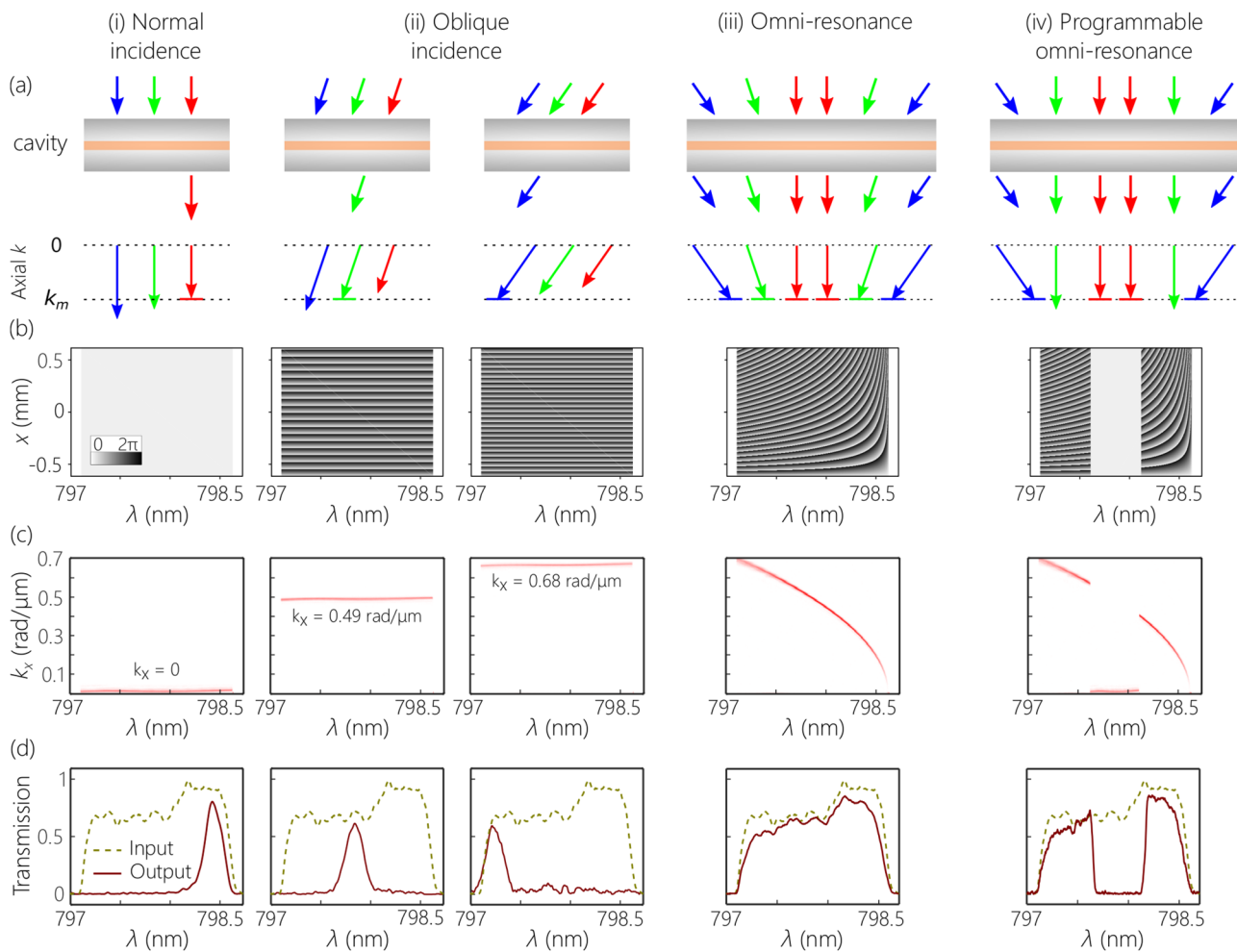
FIG. 3. Formulation of programmable omni-resonance. (a) A broad spectrum is incident on a planar FP cavity. The only wavelengths that can couple to the cavity are those whose wave vector component normal to the cavity corresponds to a resonance. (b) The phase pattern implemented on the SLM in Fig. 2(a) to produce the desired field configuration (for the sake of clarity, the plotted phase patterns here are ×2.5 larger than those implemented). (c) The measured spatiotemporal spectrum of the synthesized wave packet incident on the FP cavity and associated with the SLM phase pattern in (b). (d) Measured output spectrum after the FP cavity. The columns depict different configurations for the input field: (i) a collimated field; [(ii) and (iii)] obliquely incident fields at different angles; (iv) an omni-resonant field; and (v) a programmable omni-resonant field.

through the cavity is broad [Fig. 3(d–iii)] and matches the spectrum of the ST wave packet incident on the cavity.

The realization of programmable omni-resonance requires assigning a spatial frequency deviating from the omni-resonance condition to the wavelengths that we wish to exclude from resonating with the cavity. The wavelengths to be eliminated are thus incident on the cavity at angles incompatible with Eq. (2) [Fig. 3(a–iv)]. The phase distribution implemented by the SLM has the pattern characteristic of omni-resonant ST wave packets [Fig. 3(b–iii)] but is modified by displacing the phase at the wavelengths to be excluded [Fig. 3(b–iv)]. Consequently, the measured spatiotemporal spectrum exhibits *discontinuities* corresponding to the eliminated wavelengths [Fig. 3(c–iv)]. The cavity-transmitted spectrum of the ST wave packet matches the input spectrum except at the designated wavelengths; the transmission for wavelengths coupled to the cavity is ≈80%, while the rejected wavelengths are not detectable. By sculpting the phase distribution imparted by

the SLM to the spectrally resolved wave front, one can ensure that any prescribed spectrum be coupled to the selected cavity resonance.

V. EXAMPLES OF PROGRAMMABLE OMNI-RESONANCE

We present measurements for several examples of programmable omni-resonance. In each case, the cavity-transmitted spectrum is coupled to a multimode fiber (50-μm-diameter, 0.22-NA; Thorlabs M42L01) that delivers the signal to a high-resolution OSA (ANDO AQ6317B).

A. Controlled resonance linewidth

As a first example of programmable omni-resonance, we demonstrate controllable resonant linewidth for the cavity [Figs. 4(a)
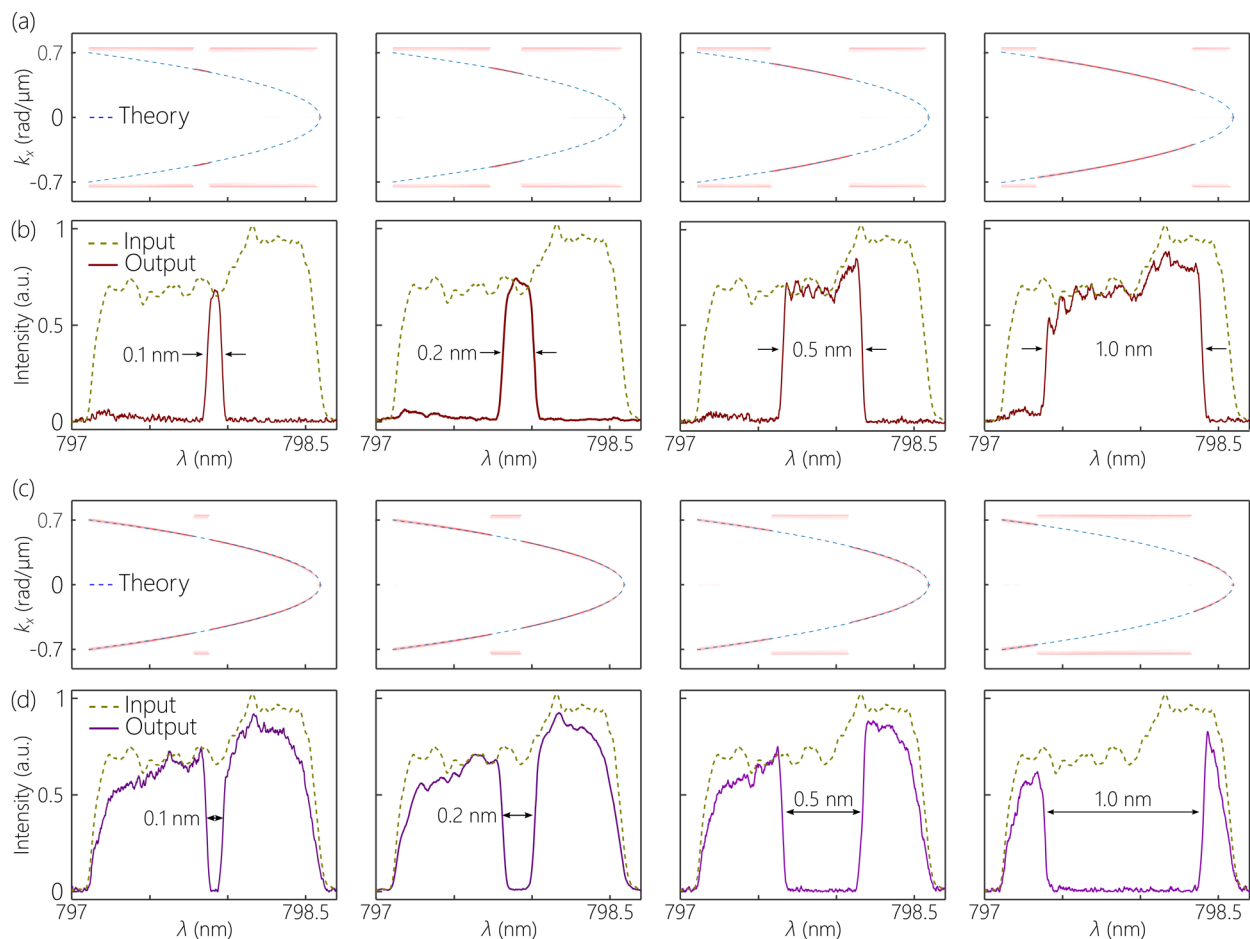
FIG. 4. [(a) and (b)] Programmable omni-resonance producing a resonant line of controllable linewidth. (a) Measured spatiotemporal spectra of the programmable omni-resonant field incident on the planar FP cavity with progressively wider bandwidth. The dotted curve is the theoretical spatiotemporal spectrum for an omni-resonant ST wave packet extending across the full system bandwidth. (b) Measured spectrum of the ST wave packet transmitted through the cavity showing a controllable-bandwidth resonant line from 0.1 nm to 1 nm. The dotted curve is the spectrum of the input field (without spatiotemporal modulation). [(c) and (d)] Same as [(a) and (b)] where programmable omni-resonance produces a spectral hole of controllable notch bandwidth in an omni-resonant background.

and 4(b)]. By eliminating all wavelengths except for a band of variable spectral width centered on a selected wavelength, one couples a controllable bandwidth to the cavity resonance. In our experiments, we confirm a resonant linewidth ranging from 0.1 nm to 1 nm. Note that one can realize a linewidth that is even *narrower* than that of the bare cavity. The extent by which we can reduce the linewidth is limited here by the spectral resolution of the wave packet synthesis arrangement in Fig. 2(a).[29] This arrangement can help extend the benefits of resonant field build-up within the cavity to large spectra unconstrained by the cavity linewidth; examples include exploiting broadband coherent perfect absorption in optical detection[30] or even in boosting the photocurrent in solar cells.[7]

B. Controlled spectral-hole bandwidth

As a second example of programmable omni-resonance, we demonstrate the complementary effect to that shown in the previous example: the entire spectrum of the incident wave packet resonates with the cavity *except* for a prescribed spectral hole [Figs. 4(b) and 4(c)]. With respect to the transmitted spectrum, the cavity is a notch filter of controllable rejection bandwidth. Here, the spatiotemporal spectrum of the ST wave packet corresponds to the omni-resonance condition in Eq. (2), except for the wavelengths that are to be rejected. These designated wavelengths are assigned to a spatial frequency that is rejected by the cavity. In Figs. 4(c) and 4(d), we produce rejected notch bandwidths ranging from 0.1 nm to 1 nm, subject to the same limitations as those of the previous example. Such a configuration enables exploiting broadband omni-resonant field enhancement of a weak field in the cavity while

excluding an unwanted strong signal, which can be useful in optical communications and optical filtering.

C. Arbitrary resonant spectral profiles

As a third example, we demonstrate arbitrary resonant spectral profiles coupled to the cavity by eliminating specific wavelengths, each associated with a selectable notch-rejection bandwidth. Alternatively, one can view the profile as the result of selecting arbitrary wavelengths to be transmitted, each associated with a tunable resonant linewidth. Two examples of such spectra are provided in Figs. 5(a) and 5(b). These two examples, along with those described above, indicate the versatility of the programmable omni-resonance strategy.

VI. SPATIOTEMPORAL CHARACTERIZATION OF PROGRAMMABLE OMNI-RESONANT SPACE–TIME WAVE PACKETS

In the examples presented above, we focused on the spectral characteristics of the transmitted programmable omni-resonant ST wave packets. Here, we shift our attention to their spatiotemporal profile. To capture time-resolved profiles of these wave packets, we make use of the interferometric configuration developed in Refs. 31 and 32 and depicted in Fig. 2(a). We place the spatiotemporal synthesis arrangement in one arm of a two-path interferometer. The original Ti:sapphire laser pulses (~100-fs pulse width) are split between the synthesis arrangement and a reference arm containing an optical delay τ. When the two wave packets (the reference pulse and the ST wave packet) overlap in space and time, spatially resolved interference fringes are observed using a CCD camera (CCD$_1$; ImagingSource, DMK 27BUP031) and an objective lens (Olympus PLN ×20) [Fig. 2(a)]. By scanning the delay in 50-μm steps, we reconstruct the spatiotemporal profile $I(x, \tau)$ of the ST wave packet transmitted through the cavity (and thus resonating with it) from the visibility of the interference fringes. Blocking the reference arm, CCD$_1$ captures the time-averaged intensity profile $I(x, y)$ at a fixed axial plane z.

With this interferometric configuration, we examine the impact of programmable omni-resonance on the spatiotemporal profile of the ST wave packet. In Fig. 6(b), we show an omni-resonant ST wave packet whose resonant bandwidth is tuned by tailoring the spatiotemporal spectrum, as shown in Fig. 6(a), using the approach developed here. When the full bandwidth resonates with the cavity, the *spatial* width of the time-averaged beam intensity is $\Delta x \approx 4.5$ μm [Fig. 6(c)]. This spatial width is inversely related to the spatial spectrum Δk_x, $\Delta x \sim \pi/\Delta k_x$, where Δk_x is also related to the bandwidth $\Delta\lambda$, as shown in Fig. 6(a). Reducing the bandwidth $\Delta\lambda$, in turn, reduces the spatial bandwidth Δk_x, which consequently increases the spatial width Δx [Fig. 6(c)].

The measured spatiotemporal profiles $I(x, \tau)$ of the ST wave packets are plotted in Fig. 6(d). We first note the X-shaped profile characteristic of ST wave packets, in general.[29,33–36] When the full spectrum resonates with the cavity (the omni-resonant configuration), we observe the smallest pulse width of ~1.5 ps in the temporal profile at the beam center $I(0, \tau)$ along with the smallest transverse spatial beam width. As we controllably reduce the resonant spectrum, the pulse width increases concomitantly with the spatial beam width.
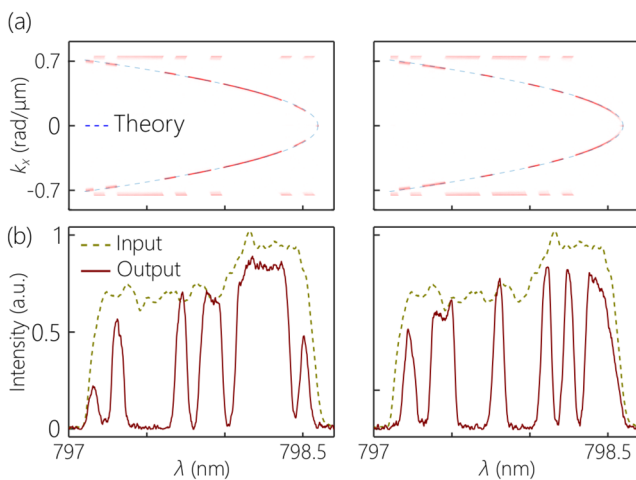
FIG. 5. Experimental realization of programmable omni-resonant spectra having arbitrary profiles. (a) Measured spatiotemporal spectra of the programmable omni-resonant field incident on the planar FP cavity. Wavelength bands are selectively excluded from the resonating spectrum. The dotted curve is the theoretical spatiotemporal spectrum for an omni-resonant ST wave packet extending across the full system bandwidth. (b) Measured spectra transmitted through the cavity for two configurations producing arbitrarily selected output spectral profiles. The dotted curve is the spectrum of the input field (without spatiotemporal modulation).
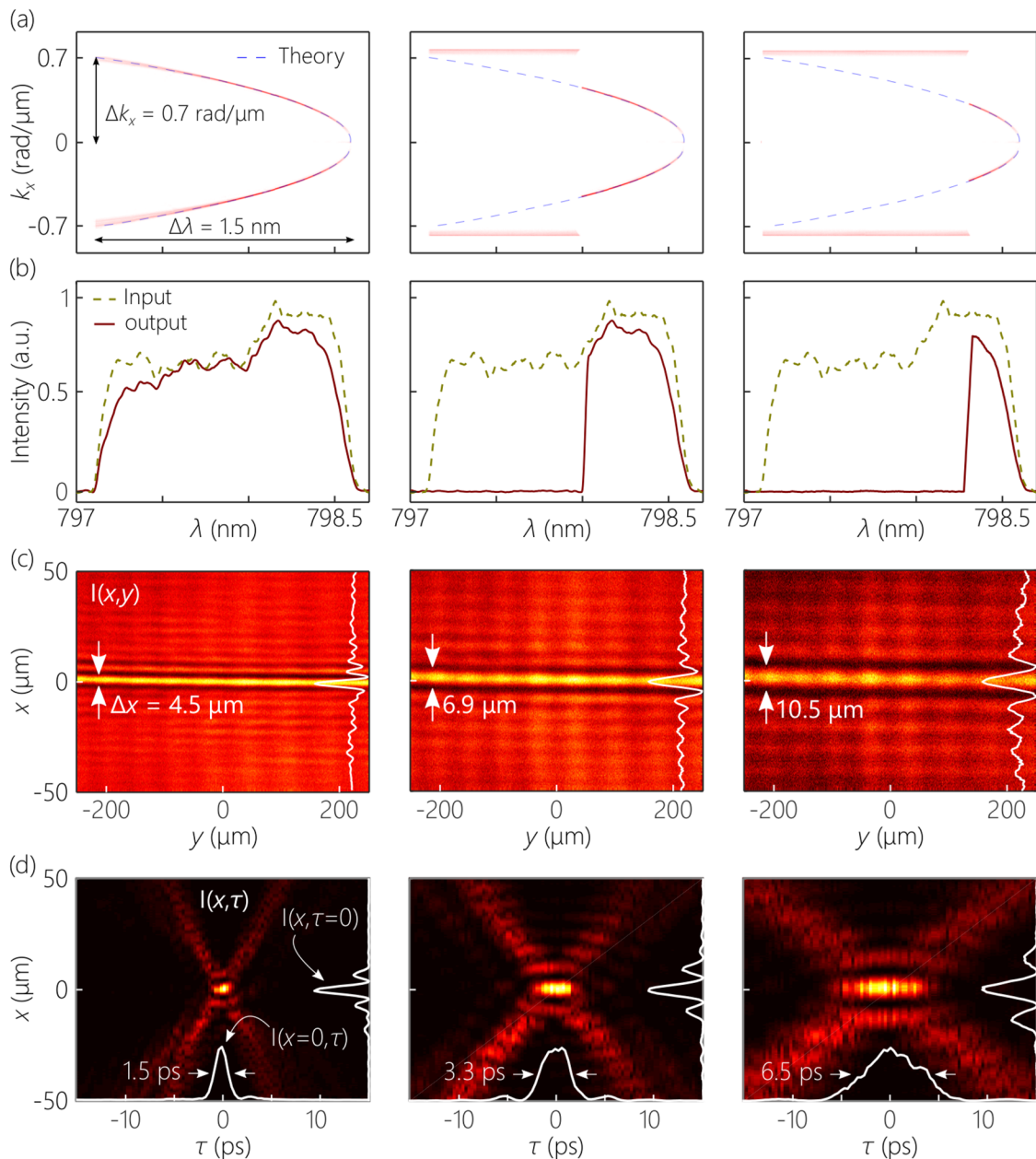
FIG. 6. Spatiotemporal characterization of programmable omni-resonant ST wave packets. (a) Measured spatiotemporal spectrum of the programmable omni-resonant ST wave packet. The dashed curve is the spatiotemporal dispersion relationship of the cavity resonance. By displacing the spatial frequency $k_x(\lambda)$ associated with any wavelength away from this dispersion curve, this wavelength fails to resonate with the cavity. From left to right, we reduce the omni-resonance bandwidth. (b) The measured cavity-transmitted spectrum compared to the spectrum of the ST wave packet incident on the cavity. (c) The measured transverse spatial profile $I(x, y)$ of the ST wave packet *after* the FP cavity. Because we have manipulated the spatial frequencies k_x along x alone, the profile takes the form of a light sheet that is uniform along y. (d) The spatiotemporal profile $I(x, \tau)$ of the ST wave packet measured after the cavity showing a characteristic X-shaped profile. The white curve along the horizontal axis in each panel is the temporal profile at the beam center $I(0, \tau)$, while the white curve along the vertical axis is the spatial profile at the pulse center $I(x, 0)$.

VII. CONCLUSION

Spatially structured light, as in the case of orbital angular momentum (OAM)[37,38] for instance, can impact the mechanical interaction of light with matter[39] and help increase optical communications rates.[40] *Temporal* pulse shaping[41,42] can help in high-speed optical communications,[43] optimizing nonlinear interactions,[44,45] and controlling chemical reactions.[46] Here, we have shown that

structuring the optical field *jointly* in space and time enables new classes of interaction with optical cavities that cannot be achieved when either spatial or temporal shaping alone is employed. We have demonstrated experimentally that introducing a precise structure into the spatiotemporal spectrum of a ST wave packet allows a programmable spectral profile to resonate with a planar FP cavity: controllable-width resonances and spectral holes and even complex arbitrary resonant spectra. Programming the width of the resonant spectrum changes the temporal and spatial widths of the ST wave packet as a result of the tight association between its spatial and temporal spectral degrees of freedom. Note that in an omni-resonant cavity, the transmission coefficient is *uniform* across the full bandwidth because the same resonance condition is satisfied at all wavelengths. Although we have made use here of coherent pulsed fields,[28] incoherent fields can also benefit from this strategy.[47,48] Furthermore, much broader spectral bandwidths are accessible for omni-resonance than we have exploited here.[7,26,27]

This work can be viewed as a further contribution to the emerging field of space–time optics and photonics. Introducing tight spatiotemporal spectral correlations in the optical field[20,23,49] leads to new optical behavior upon free propagation such as self-healing,[50] controllable group velocity,[31,32,51–54] transverse OAM,[55] ultrafast beam steering,[56] axially accelerating and decelerating wave packets,[54] and a veiled space–time Talbot effect.[57] Moreover, ST wave packets interact with photonic devices in novel ways, including anomalous refraction,[58] new hybrid guided ST modes in unpatterned thin films that can overcome the limitations imposed by boundary conditions,[59] propagation-invariant ST surface plasmon polaritons that are confined in all dimensions,[60] and boosting the infrared photocurrent in solar cells exploiting omni-resonance.[7] The results reported here have the potential to add a new degree of freedom to applications that can make use of omni-resonance by offering access to arbitrary resonant spectral profiles.

DATA AVAILABILITY

The data that support the findings of this study are available from the corresponding author upon reasonable request.

REFERENCES

[1] B. E. A. Saleh and M. C. Teich, *Principles of Photonics* (Wiley, 2007).
[2] S. Haroche and J.-M. Raimond, *Exploring the Quantum: Atoms, Cavities, and Photons* (Oxford Univ, Oxford, 2006).
[3] Y. D. Chong, L. Ge, H. Cao, and A. D. Stone, "Coherent perfect absorbers: Time-reversed lasers," Phys. Rev. Lett. **105**, 053901 (2010).
[4] W. Wan, Y. Chong, L. Ge, H. Noh, A. D. Stone, and H. Cao, "Time-reversed lasing and interferometric control of absorption," Science **331**, 889–892 (2011).
[5] M. L. Villinger, M. Bayat, L. N. Pye, and A. F. Abouraddy, "Analytical model for coherent perfect absorption in one-dimensional photonic structures," Opt. Lett. **40**, 5550–5553 (2015).
[6] D. G. Baranov, A. Krasnok, T. Shegai, A. Alú, and Y. Chong, "Coherent perfect absorbers: Linear control of light with light," Nat. Rev. Mater. **2**, 17064 (2017).
[7] M. L. Villinger, A. Shiri, S. Shabahang, A. K. Jahromi, M. B. Nasr, C. Villinger, and A. F. Abouraddy, "Doubling the near-infrared photocurrent in a solar cell via omni-resonant coherent perfect absorption," arXiv:1911.09276 (2019).
[8] M. Soljačić and J. D. Joannopoulos, "Enhancement of nonlinear effects in photonic crystals," Nat. Mater. **3**, 211–219 (2004).
[9] E. Makri, H. Ramezani, T. Kottos, and I. Vitebskiy, "Concept of a reflective power limiter based on nonlinear localized modes," Phys. Rev. A **89**, 031802(R) (2014).
[10] Z. Lin, X. Liang, M. Lončar, S. G. Johnson, and A. W. Rodriguez, "Cavity-enhanced second-harmonic generation via nonlinear-overlap optimization," Optica **3**, 233–238 (2016).
[11] J. H. Vella, J. H. Goldsmith, A. T. Browning, N. I. Limberopoulos, I. Vitebskiy, E. Makri, and T. Kottos, "Experimental realization of a reflective optical limiter," Phys. Rev. Appl. **5**, 064010 (2016).
[12] M. Minkov, D. Gerace, and S. Fan, "Doubly resonant $\chi^{(2)}$ nonlinear photonic crystal cavity based on a bound state in the continuum," Optica **6**, 1039–1045 (2019).
[13] A. Wicht, K. Danzmann, M. Fleischhauer, M. Scully, G. Müller, and R.-H. Rinkleff, "White-light cavities, atomic phase coherence, and gravitational wave detectors," Opt. Commun. **134**, 431–439 (1997).
[14] G. S. Pati, M. Salit, K. Salit, and M. S. Shahriar, "Demonstration of a tunable-bandwidth white-light interferometer using anomalous dispersion in atomic vapor," Phys. Rev. Lett. **99**, 133601 (2007).
[15] H. Wu and M. Xiao, "White-light cavity with competing linear and nonlinear dispersions," Phys. Rev. A **77**, 031801(R) (2008).
[16] H. N. Yum, J. Scheuer, M. Salit, P. R. Hemmer, and M. S. Shahriar, "Demonstration of white light cavity effect using stimulated Brillouin scattering in a fiber loop," J. Lightwave Technol. **31**, 3865–3872 (2013).
[17] S. Wise, V. Quetschke, A. J. Deshpande, G. Mueller, D. H. Reitze, D. B. Tanner, B. F. Whiting, Y. Chen, A. Tünnermann, E. Kley, and T. Clausnitzer, "Phase effects in the diffraction of light: Beyond the grating equation," Phys. Rev. Lett. **95**, 013901 (2005).
[18] H. N. Yum, X. Liu, P. R. Hemmer, J. Scheuer, and M. S. Shahriar, "The fundamental limitations on the practical realizations of white light cavities," Opt. Commun. **305**, 260–266 (2013).
[19] J. P. Torres, M. Hendrych, and A. Valencia, "Angular dispersion: An enabling tool in nonlinear and quantum optics," Adv. Opt. Photonics **2**, 319–369 (2010).
[20] H. E. Kondakci and A. F. Abouraddy, "Diffraction-free pulsed optical beams via space-time correlations," Opt. Express **24**, 28659–28668 (2016).
[21] K. J. Parker and M. A. Alonso, "The longitudinal iso-phase condition and needle pulses," Opt. Express **24**, 28669–28677 (2016).
[22] H. E. Kondakci and A. F. Abouraddy, "Diffraction-free space-time beams," Nat. Photonics **11**, 733–740 (2017).
[23] M. Yessenov, B. Bhaduri, H. E. Kondakci, and A. F. Abouraddy, "Classification of propagation-invariant space-time light-sheets in free space: Theory and experiments," Phys. Rev. A **99**, 023856 (2019).
[24] M. Yessenov, B. Bhaduri, H. E. Kondakci, and A. F. Abouraddy, "Weaving the rainbow: Space-time optical wave packets," Opt. Photonics News **30**, 34–41 (2019).
[25] R. Donnelly and R. W. Ziolkowski, "Designing localized waves," Proc. R. Soc. London, Ser. A **440**, 541–565 (1993).
[26] S. Shabahang, H. E. Kondakci, M. L. Villinger, J. D. Perlstein, A. El Halawany, and A. F. Abouraddy, "Omni-resonant optical micro-cavity," Sci. Rep. **7**, 10336 (2017).
[27] S. Shabahang, A. K. Jahromi, A. Shiri, K. L. Schepler, and A. F. Abouraddy, "Toggling between active and passive imaging with an omni-resonant micro-cavity," Opt. Lett. **44**, 1532–1535 (2019).
[28] A. Shiri, M. Yessenov, R. Aravindakshan, and A. F. Abouraddy, "Omni-resonant space-time wave packets," Opt. Lett. **45**, 1774–1777 (2020).
[29] M. Yessenov, B. Bhaduri, L. Mach, D. Mardani, H. E. Kondakci, M. A. Alonso, G. A. Atia, and A. F. Abouraddy, "What is the maximum differential group delay achievable by a space-time wave packet in free space?," Opt. Express **27**, 12443–12457 (2019).

[30] L. N. Pye, M. L. Villinger, S. Shabahang, W. D. Larson, L. Martin, and A. F. Abouraddy, "Octave-spanning coherent absorption in a thin silicon film," Opt. Lett. **42**, 151–154 (2017).

[31] H. E. Kondakci and A. F. Abouraddy, "Optical space-time wave packets of arbitrary group velocity in free space," Nat. Commun. **10**, 929 (2019).

[32] B. Bhaduri, M. Yessenov, and A. F. Abouraddy, "Space-time wave packets that travel in optical materials at the speed of light in vacuum," Optica **6**, 139–146 (2019).

[33] P. Saari and K. Reivelt, "Evidence of X-shaped propagation-invariant localized light waves," Phys. Rev. Lett. **79**, 4135–4138 (1997).

[34] K. Reivelt and P. Saari, "Localized wave solutions of the scalar homogeneous wave equation and their optical implementation," arXiv:physics/0309079 (2003).

[35] J. Turunen and A. T. Friberg, "Propagation-invariant optical fields," Prog. Opt. **54**, 1–88 (2010).

[36] *Non-Diffracting Waves*, edited by H. E. Hernández-Figueroa, E. Recami, and M. Zamboni-Rached (Wiley-VCH, 2014).

[37] L. Allen, M. W. Beijersbergen, R. J. C. Spreeuw, and J. P. Woerdman, "Orbital angular momentum of light and the transformation of Laguerre-Gaussian laser modes," Phys. Rev. A **45**, 8185–8189 (1992).

[38] A. M. Yao and M. J. Padgett, "Orbital angular momentum: Origins, behavior and applications," Adv. Opt. Photonics **3**, 161–204 (2011).

[39] N. B. Simpson, K. Dholakia, L. Allen, and M. J. Padgett, "Mechanical equivalence of spin and orbital angular momentum of light: An optical spanner," Opt. Lett. **22**, 52–54 (1997).

[40] J. Wang, J.-Y. Yang, I. M. Fazal, N. Ahmed, Y. Yan, H. Huang, Y. Ren, Y. Yue, S. Dolinar, M. Tur, and A. E. Willner, "Terabit free-space data transmission employing orbital angular momentum multiplexing," Nat. Photonics **6**, 488–496 (2012).

[41] A. M. Weiner, "Femtosecond pulse shaping using spatial light modulators," Rev. Sci. Instrum. **71**, 1929–1960 (2000).

[42] A. M. Weiner, *Ultrafast Optics* (John Wiley & Sons, Inc., 2009).

[43] H. P. Sardesai, C.-C. Chang, and A. M. Weiner, "A femtosecond code-division multiple-access communication system test bed," J. Lightwave Technol. **16**, 1953–1964 (1998).

[44] D. Meshulach and Y. Silberberg, "Coherent quantum control of two-photon transitions by a femtosecond laser pulse," Nature **396**, 239–242 (1998).

[45] D. Meshulach and Y. Silberberg, "Coherent quantum control of multiphoton transitions by shaped ultrashort optical pulses," Phys. Rev. A **60**, 1287–1292 (1999).

[46] A. Assion, T. Baumert, M. Bergt, T. Brixner, B. Kiefer, V. Seyfried, M. Strehle, and G. Gerber, "Control of chemical reactions by feedback-optimized phase-shaped femtosecond laser pulses," Science **282**, 919–922 (1998).

[47] M. Yessenov, B. Bhaduri, H. E. Kondakci, M. Meem, R. Menon, and A. F. Abouraddy, "Non-diffracting broadband incoherent space–time fields," Optica **6**, 598 (2019).

[48] M. Yessenov and A. F. Abouraddy, "Changing the speed of coherence in free space," Opt. Lett. **44**, 5125–5128 (2019).

[49] H. E. Kondakci, M. A. Alonso, and A. F. Abouraddy, "Classical entanglement underpins the invariant propagation of space–time wave packets," Opt. Lett. **44**, 2645–2648 (2019).

[50] H. E. Kondakci and A. F. Abouraddy, "Self-healing of space-time light sheets," Opt. Lett. **43**, 3830–3833 (2018).

[51] A. Sainte-Marie, O. Gobert, and F. Quéré, "Controlling the velocity of ultrashort light pulses in vacuum through spatio-temporal couplings," Optica **4**, 1298–1304 (2017).

[52] D. H. Froula, D. Turnbull, A. S. Davies, T. J. Kessler, D. Haberberger, J. P. Palastro, S.-W. Bahk, I. A. Begishev, R. Boni, S. Bucht, J. Katz, and J. L. Shaw, "Spatiotemporal control of laser intensity," Nat. Photonics **12**, 262–265 (2018).

[53] S. W. Jolly, O. Gobert, A. Jeandet, and F. Quéré, "Controlling the velocity of a femtosecond laser pulse using refractive lenses," Opt. Express **28**, 4888–4897 (2020).

[54] M. Yessenov and A. F. Abouraddy, "Accelerating and decelerating space-time optical wave packets in free space," arXiv:2004.00380 (2020).

[55] A. Chong, C. Wan, J. Chen, and Q. Zhan, "Generation of spatiotemporal optical vortices with controllable transverse orbital angular momentum," Nat. Photonics **14**, 350 (2020).

[56] A. M. Shaltout, K. G. Lagoudakis, J. van de Groep, S. J. Kim, J. Vučković, V. M. Shalaev, and M. L. Brongersma, "Spatiotemporal light control with frequency-gradient metasurfaces," Science **365**, 374–377 (2019).

[57] M. Yessenov, L. A. Hall, S. A. Ponomarenko, and A. F. Abouraddy, "Veiled space-time Talbot effect," arXiv:2004.04875 (2020).

[58] B. Bhaduri, M. Yessenov, and A. F. Abouraddy, "Anomalous refraction of optical spacetime wave packets," Nat. Photon. **14**, 416–421 (2020).

[59] A. Shiri, M. Yessenov, S. Webster, K. L. Schepler, and A. F. Abouraddy, "Hybrid guided space-time optical modes in unpatterned films," arXiv:2001.01991 (2020).

[60] K. L. Schepler, M. Yessenov, Y. Zhiyenbayev, and A. F. Abouraddy, "Space-time surface plasmon polaritons: A new propagation-invariant surface wave packet," arXiv:2003.02105 (2020).